Prediction of Mechanical Properties of Fused Deposition Modeling Made Parts using Multiscale Modeling and Classical Laminate Theory

A. Nasirov*, S. Hasanov*, I. Fidan[¥]

*Department of Mechanical Engineering and Center for Manufacturing Research
[¥]Department of Manufacturing and Engineering Technology
College of Engineering
Tennessee Technological University
Cookeville, TN 38505

Abstract

Fused deposition modeling (FDM) is one of the most popular additive manufacturing (AM) processes that works based on the layer-by-layer buildup of a 3D modeled part from polymers or fiber-reinforced polymer materials. In recent years, extensive research has been done to characterize the mechanical properties of FDM produced parts using classical laminate theory (CLT). However, considering the limitation of micromechanics approach to simple unit cells, there is a need to explore different techniques to alleviate those limitations. Taking into account the periodicity and multiscale nature of FDM infill patterns, one such technique is the asymptotic homogenization method used in this study to find mechanical properties. Moreover, the input of homogenized properties in CLT is discussed. Finally, both homogenization and CLT results are compared with experimental results.

1. Introduction

As 3D Printing becomes more popular in the industry, characterization of mechanical properties of 3D printed parts becomes a point of interest to many engineers. However, elastic constants are very hard to determine due to a number of reasons. First of all, FDM manufactured parts are anisotropic due to different building direction of layers. Furthermore, process parameters, such as layer thickness, air gap, etc., affect mechanical properties since there are voids inside the part. At last, surface and internal defects have a negative effect on the strength of the 3D printed parts. An example of surface defects is staircase error which happens when 3D printer approximates external curves. An example of internal defects is internal voids inside the part because of the toolpath specifications [1].

A review paper by Cuan-Urquizo et al. presents an overview of different experimental, computational and analytical methods used so far [2]. Domingo-Espin et al. assumed that printed parts are assumed to be orthotropic instead of anisotropic [3]. Even though this is a fair approximation in the elastic region and low deformations, it requires lots of testing to be performed and does not yield any information about the mechanics of the parts. Li et al. treated each layer as a lamina consisting of beads and fibers and voids as a matrix [4]. Although there were instances where theoretical and experimental results did not match (due to assumptions in analytical calculations), overall, the work was successful in predicting elastic constants theoretically. Somireddy et al., performed finite element analysis (FEA) on the mesostructure level to determine strain energy and then laminate elastic properties [5]. Rodriguez et al. derived and applied micromechanics approach for constitutive modeling of FDM made parts [6]. Derived equations yield simple approximations for mechanical constants and can be used by engineers for rough

calculations. Croccolo et al. utilized an analytical model to predict the mechanical properties with zero air gap between the beads [7]. The inclined beads were assumed to behave as an inclined truss member. Based on his results, there was an approximately 4% difference in predicted stiffness and strength values with respect to experimental results. The model used in his study is excellent in predicting the stiffness of the samples but is also restricted to 100% density. Huang and Singamneni et al. investigated the effective stiffness and strength properties of unidirectional test specimens printed with different raster angles [8]. In-plane stress and perfectly bonded layers are assumed in the analytical model. In a different study, they considered the bead cross-sections to be square with elliptical fillets. As a result of the findings, the coalescence between layers is found to be sensitive. Cuan-Urquizo et al. studied the effective properties of the printed part with the presence of voids in the printed structures [9]. The unit cell consisted of cellular material and was treated as lattice structure. Lattice was considered to be loaded along one of the main axes with beads parallel to the loading direction. Mechanical properties were derived based on the rule of mixtures. The relative error between effective properties and finite element predictions was less than 10%.

One of the most common infill patterns is line or rectilinear infill. Line infill can be customized to print each layer in a different direction. This project investigates the application of multiscale modeling as a constitutive modeling tool for parts made with the line infill. Asymptotic homogenization (AH) is one of the multiscale modeling techniques that is used for the parts with periodic microstructures. The main objective of the work is to investigate homogenization approach as a tool for predicting mechanical properties of FDM-printed parts and investigate post-processing possibility of microscale displacements, strains, and stresses. Experimental results are used for validation of theoretical results. However, tensile experiments can only be performed for balanced symmetric laminates due to tensions-shear, tension-bending, and tension-torsion coupling. Therefore, the two cases discussed here are all-zero layup and 0/90 layup. Moreover, ideal and actual representative volume elements (RVEs) are used in the study to assess the influence of the microstructure on the mechanical behavior. Moreover, results from CLT are used to predict 0/90 layup properties from all-zero degree layup. Finally, homogenization and CLT results are compared to experimental results.

2. Materials and Methods

2.1.Asymptotic Homogenization Theory

Palencia [10], and Guedes and Kikuchi [11] developed asymptotic homogenization, a mathematical theory that homogenizes heterogeneous parts based on the asymptotic expansion of displacement field (**u**) over macro and microscale domains. The mathematical formulation is as follows:

$$\boldsymbol{u}(\boldsymbol{x}) \approx \boldsymbol{u}^{\epsilon}(\boldsymbol{x},\boldsymbol{y}) = \boldsymbol{u}^{(0)} + \epsilon\boldsymbol{u}^{(1)} + \epsilon^{2}\boldsymbol{u}^{(2)} + \cdots \quad (1)$$

where $\boldsymbol{y}$ is the microscale coordinate vector defined on RVE domain and $\boldsymbol{x}$ is the macroscale coordinate vector defined over continuum body**.** RVE is a self-repeating element that is selected from the microstructure of the macroscale part. Plugging expanded displacement field in linear strain $\boldsymbol{\varepsilon^{\epsilon}}$ and stress tensors $\boldsymbol{\sigma^{\epsilon}}$**,** the following equations are obtained:

$$\boldsymbol{\varepsilon}^{\epsilon}(\boldsymbol{x},\boldsymbol{y}) = \frac{1}{\epsilon}\boldsymbol{\varepsilon}^{(-1)} + \boldsymbol{\varepsilon}^{(0)} + \epsilon\boldsymbol{\varepsilon}^{(1)} + \cdots \quad (2)$$

$$\boldsymbol{\sigma}^{\epsilon}(\boldsymbol{x},\boldsymbol{y}) = \frac{1}{\epsilon}\boldsymbol{\sigma}^{(-1)} + \boldsymbol{\sigma}^{(0)} + \epsilon\boldsymbol{\sigma}^{(1)} + \cdots \quad (3)$$

Using the equations given above in a static elasticity equation, terms with the same ϵ order are grouped and equated to zero. The further derivation is omitted here for the sake of brevity. For a detailed discussion of asymptotic homogenization theory, the reader is referred to [10–13]. As a result of the derivation, we obtain a partial differential equation (PDE) given in equation (4) representing microscale equilibrium over Y (RVE domain) with periodic boundary conditions and additional constraint equation to enforce zero mean of displacement influence function and guarantee uniqueness of the solution.

$$[C_{ijkl}(H^{mn}_{(k,y_l)} + I_{klmn})]_{,y_j} = 0 \; on \; Y \tag{4}$$

$$H^{mn}_k(\boldsymbol{y}) = H^{mn}_k(\boldsymbol{y} + \boldsymbol{l}) \; on \; \partial Y$$

$$subject \; to \;\; \int H^{mn}_k \, dY = 0$$

where C_{ijkl} is stiffness tensor of pure material, H^{mn}_k is displacement influence function, I_{ijkl} is fourth-order identity tensor. Homogenized stiffness tensor, D_{ijmn}, can be calculated using equation (5).

$$D_{ijmn} = \int (C_{ijmn} + C_{ijkl} H^{mn}_{(k,y_l)}) \, dY / |Y| \tag{5}$$

The extracted homogenized constants are used in a macroscale finite element model that is solved for the macroscale displacement field $\boldsymbol{u}^{(0)}$ on the tensile specimen geometry. One side of the specimen is fixed and the other one is loaded with traction vector corresponding to maximum force sustained during the tensile test. Finally, AH makes it possible to calculate deformations, strains, and stresses at the microscale in the post-processing stage. The mesh is imported to an in-house built MATLAB code that solves both micro and macro-scale equations and exports results in Paraview visualization software. Overall, the algorithm followed in this paper is illustrated in

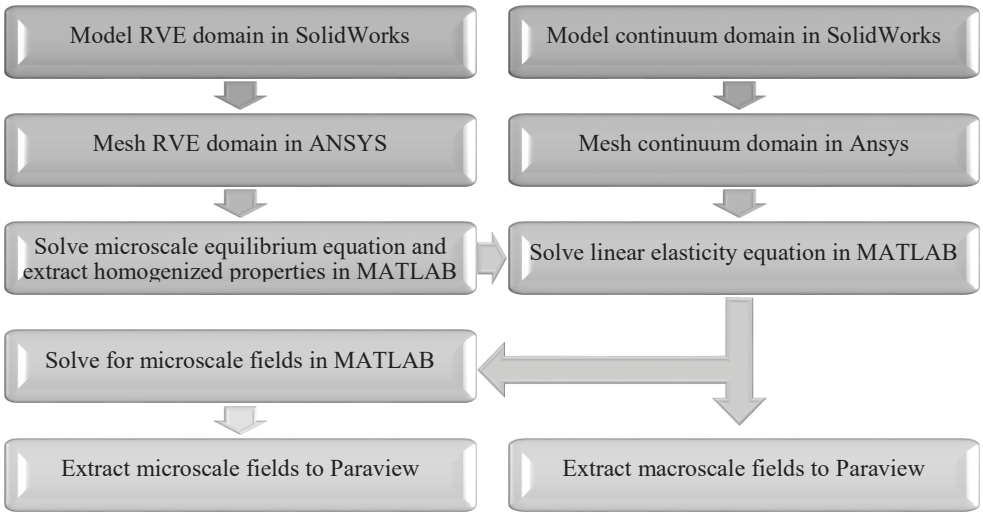

Figure 1. The workflow of the homogenization procedure

Fig. 1. Both RVE and continuum scale geometries are modeled in SolidWorks and then imported to ANSYS for meshing.

2.2. CLT

Next, predicted mechanical properties from the all-zero case are used in CLT to predict properties of the whole laminate in 0/90 case. In general, CLT is widely used for modeling mechanical behavior of laminated composite plates. CLT is centered around "ABD matrix" that relates strains and curvatures to forces and moments as illustrated in equation (6).

$$\begin{Bmatrix} N \\ M \end{Bmatrix} = \begin{bmatrix} A & B \\ B & D \end{bmatrix} \begin{Bmatrix} \varepsilon \\ k \end{Bmatrix} \tag{6}$$

where N is force vector, M is moment vector, ε is strain vector, k is curvature vector, $A = \sum_{k=0}^{n} Q(\theta_k)\,(z_k - z_{k-1})$, $B = \frac{1}{2}\sum_{k=0}^{n} Q(\theta_k)\,(z_k^2 - z_{k-1}^2)$, and $D = \frac{1}{3}\sum_{k=0}^{n} Q(\theta_k)\,(z_k^3 - z_{k-1}^3)$. For symmetric laminates, B matrix is equal to zero matrix and for balanced laminates there is no tension-shear coupling in A matrix (A_{16}= A_{26}=0). Since 0/90 layup is both balanced and symmetric both of these properties hold. Therefore, smeared mechanical properties of the laminate can be calculated by inverting A matrix and then extracting Young modulus and Poisson's ratio from compliance matrix divided by the thickness of the laminate.

2.3.Experimental Setup

In this study, specimens were printed with the polylactic acid (PLA) using Ultimaker 2+ Extended with printing settings given in Table 1. Settings that are not mentioned here are given by default in slicing software (in this case Cura). Shells, top and bottom layers have been omitted to exclude their effect on homogenization results.

Table 1. Printing Settings

Printing parameter	Setting
Material	PLA
Nozzle diameter (mm)	0.4
Infill pattern	Line
Infill density (%)	100
Nozzle temperature (^{0}C)	215
Bed temperature (^{0}C)	50
Printing speed (mm/s)	50
Layer height (mm)	0.2
Number of shells/top/bottom layers	0
Cooling fan (%)	100

To validate theoretical results obtained from homogenization and to get a better insight into the mechanical behavior of the grid pattern, tensile tests were performed. Testing was conducted in accordance with ASTM D638 "Standard Test Method for Tensile Properties of Plastics". Strain rate during the test was 5 mm/min. Testing was done using Instron 5582 UTM.

Table 2. Experimental results

Testing Direction/ Layup	Young Modulus (Pa)		Yield Strength (Pa)	
	Mean	Deviation	Mean	Deviation
0/	3.067E+09	3.27E+07	5.059E+07	9.75E+05
90/	2.353E+09	7.63E+07	2.103E+07	5.95E+05
V	2.064E+09	1.51E+08	1.882E+07	3.18E+06
0/90	2.835E+09	5.56E+07	3.773E+07	8.40E+05
90/0	2.791E+09	1.38E+08	3.611E+07	8.44E+05
0/90/V	2.653E+09	2.45E+08	2.608E+07	5.73E+06

Two cases of laminate layup were assessed all-zero and zero-ninety. Since this study attempts to predict mechanical properties in different directions, specimens were printed with following layups all-zero (0), all-ninety (90), all-zero vertical (0V), zero-ninety (0-90), ninety-zero (90-0) and zero-ninety vertical (0-90V). Specimen name coding is explained in Figure 2 with testing and printing directions are shown using arrows.

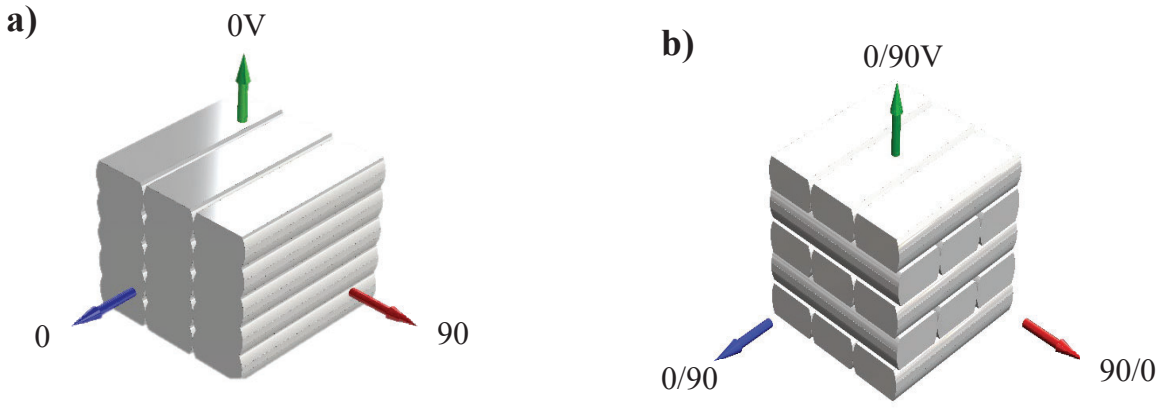

Figure 2. Specimen Coding Explained: a) All-zero b) 0/90 layup

3. Results & discussion

3.1. Experimental Results

Experimental results are summarized in Table 2. Results are classified according to specimen code. Young modulus, maximum force and tensile strength of the tested samples are reported. Overall, material behavior was brittle with almost no yielding/plastic deformation upon fracture. 0-degree layup is stronger and stiffer in 0-degree than in 90-degree as expected. The vertical direction is weaker than both 0 and 90 directions. The same pattern is observed in the tensile strength of 0/90 degree layup.

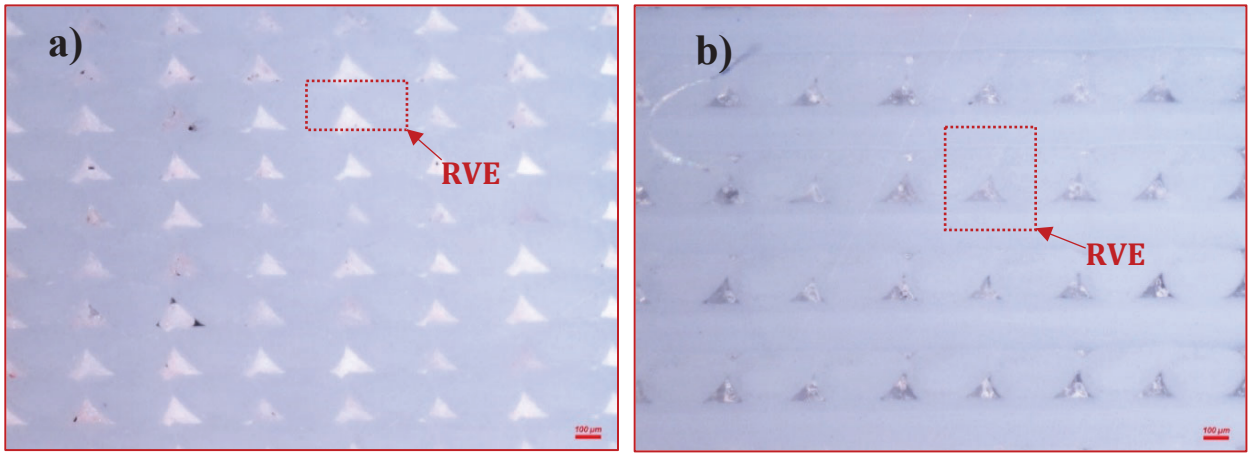

Figure 3. Microstructural Images a) All-zero b) 0/90 layup

3.2.Homogenization & CLT

The first step in the homogenization procedure is RVE selection from microstructural images given in Fig. 3a, b. RVE showed in Fig. 3a will be used for homogenization prediction of the 0-degree layup. Furthermore, RVE presented in Fig. 3b will be used to predict properties of the 0/90 layup straight from asymptotic homogenization and then results from homogenization prediction of all-zero layup will be used in CLT to predict smeared laminate properties.

Furthermore, two cases for the RVEs will be considered: ideal and actual (taken from microstructure). Ideal RVE is the one presented in the slicer software. Beads were approximated as ellipses with bead width and layer height given in slicer software, and ellipse minor axis was assumed to be equal to 0.4 mm (nozzle diameter). Actual RVE was reconstructed from optical microscope images using ImageJ image processing software. All four RVE cases are shown in Fig. 4.

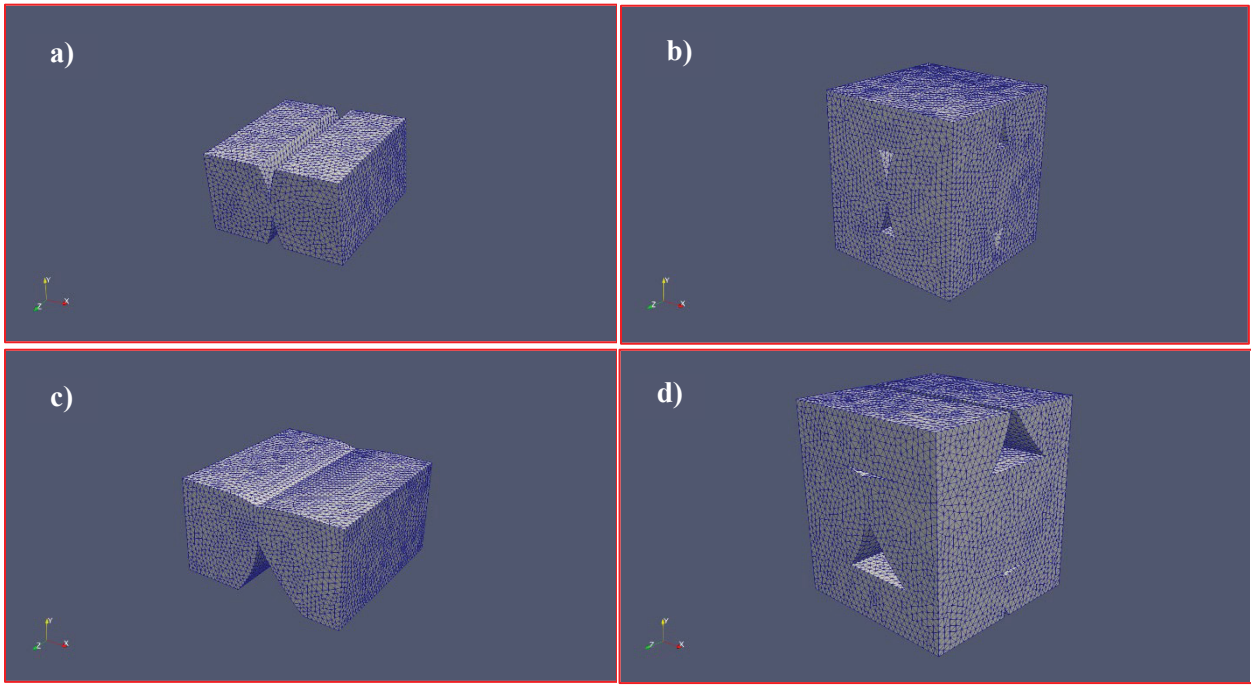

Figure 4. a) Ideal RVE b) Full Ideal RVE c) Actual RVE d) Full Actual RVE

Homogenization was performed on ideal and actual RVEs, presented in Fig. 4a and c, to extract properties for 0 and 90-degree layups. It should be noted that the homogenized stiffness matrix is anisotropic for both ideal and actual RVE cases. However, orthotropic terms are 10^3 order higher than the rest of the terms for ideal RVE. Therefore, it is safe to assume that the material constitutive model is orthotropic. In the case of actual RVE, the stiffness matrix is given in equation (7) below. As the matrix shows $D(6,1:3)$ terms are close to the orthotropic terms. Therefore, material behavior resembles that of monoclinic material. The study will still proceed with the derivation of orthotropic constants simplifying material behavior.

$$D_{ijkl} = \begin{bmatrix} 2.902 * 10^9 & SYM & SYM & SYM & SYM & SYM \\ 1.181 * 10^9 & 3.242 * 10^9 & SYM & SYM & SYM & SYM \\ 1.469 * 10^8 & 1.592 * 10^9 & 4.201 * 10^9 & SYM & SYM & SYM \\ 1.943 * 10^5 & 1.432 * 10^5 & 3.069 * 10^5 & 9.734 * 10^8 & SYM & SYM \\ 3.478 * 10^5 & -7.585 * 10^2 & 1.764 * 10^5 & -2.581 * 10^7 & 9.137 * 10^8 & SYM \\ -1.374 * 10^8 & -8.852 * 10^7 & -8.127 * 10^7 & -1.357 * 10^5 & -2.250 * 10^5 & 7.901 * 10^8 \end{bmatrix} Pa \quad (7)$$

Homogenization results are compared to experimental ones in Table 3. As Table 3 suggests ideal RVE Young modulus prediction has low relative errors in 0 and 90 directions and high relative error in a vertically printed sample. Results based on actual RVE have lower errors in 0 and 0V cases with a slight increase in 90 case. However, error in vertically printed specimens is still high even for actual RVE. A possible reason for this might be imperfect bonding between the layers. As results show actual RVE has much lower errors both for homogenization approaches.

Table 3. Young moduli comparison: Experimental vs Homogenization

Specimen Code	Experimental Young Modulus (Pa)	Homogenization			
		Ideal RVE	Error	Actual RVE	Error
0	3.067E+09	3.349E+09	9.222	3.102E+09	1.159
90	2.353E+09	2.210E+09	-6.066	2.197E+09	-6.629
0V	2.064E+09	3.287E+09	59.241	2.453E+09	18.819

The same procedure was performed for the 0/90 layup case. However, this time two different methodologies were used as shown. First one is homogenization which refers to RVE given in Fig 4b and d, this RVEs allow prediction of 0/90 degree layup straight from homogenization. Moreover, homogenization results from all-zero layup were used in CLT and then laminate smeared properties were calculated. Results of the calculations are compared with experimental results in Table 4. The homogenized stiffness matrix for ideal RVE followed a similar trend as before and for actual RVE case is shown in equation (8) below. It is evident that there are even more coupling terms that have magnitude comparable to orthotropic terms.

$$D_{ijkl} = \begin{bmatrix} 3.330 * 10^9 & SYM & SYM & SYM & SYM & SYM \\ 9.668 * 10^8 & 2.252 * 10^9 & SYM & SYM & SYM & SYM \\ 1.282 * 10^9 & 9.643 * 10^8 & 3.321 * 10^9 & SYM & SYM & SYM \\ 2.674 * 10^7 & 2.603 * 10^7 & 5.397 * 10^7 & 7.575 * 10^8 & SYM & SYM \\ -1.297 * 10^6 & -6.957 * 10^5 & -1.327 * 10^6 & -9.697 * 10^6 & 9.297 * 10^8 & SYM \\ -5.254 * 10^7 & -2.553 * 10^7 & -2.586 * 10^7 & -4.097 * 10^5 & 9.720 * 10^6 & 7.588 * 10^8 \end{bmatrix} Pa \quad (8)$$

As in the previous case, the highest errors are observed for vertically printed samples as shown in Table 4. For 0/90 and 90/0 cases relative errors are low. Young modulus in 0/90 case is slightly higher than 90/0 case because there is one more 0-degree layer (90-degree in 90/0 case). Relative errors are under 8% for homogenization in 0/90 and 90/0 directions. Actual RVE improves error in 90/0 degree considerably but increases error in the vertical direction. In CLT case, Actual RVE performs great in all three cases while Ideal RVE has relatively large error in the vertical direction. As results suggest, actual RVE coupled with CLT has relative errors lower than 8 % while other configurations underperform in vertical direction.

Table 4. Young moduli comparison: Experimental vs Homogenization

Specimen Code	Experimental Young Modulus (Pa)	Homogenization				CLT			
		Ideal RVE	Error	Actual RVE	Error	Ideal RVE	Error	Actual RVE	Error
0/90	2.835E+09	2.976E+09	4.978	2.625E+09	-7.396	2.84E+09	0.347	2.702E+09	4.674
90/0	2.791E+09	2.976E+09	6.628	2.625E+09	-5.956	2.80E+09	0.277	2.666E+09	4.479
0/90V	2.653E+09	3.182E+09	19.942	1.764E+09	-33.531	3.29E+09	23.894	2.454E+09	7.512

3.3 Microscale normalized stress fields

Finally, microscale stress fields are shown on actual RVE for all-zero case (but can be calculated for all cases). Microscale normalized stresses are shown on the RVE domain for two loading cases as shown in Figure 5. Yellow arrows illustrate loading direction. Although stress values increase unboundedly at sharp corners (due to singularity), both far-field and near-field stress values can be visualized under different loading conditions. Therefore, engineers can potentially predict where material is going to fail on the microscale. It should be noted that stress values were post-processed by averaging over the Gaussian quadrature points. Stress values presented are derived according to normal stress theory since PLA is a brittle material.

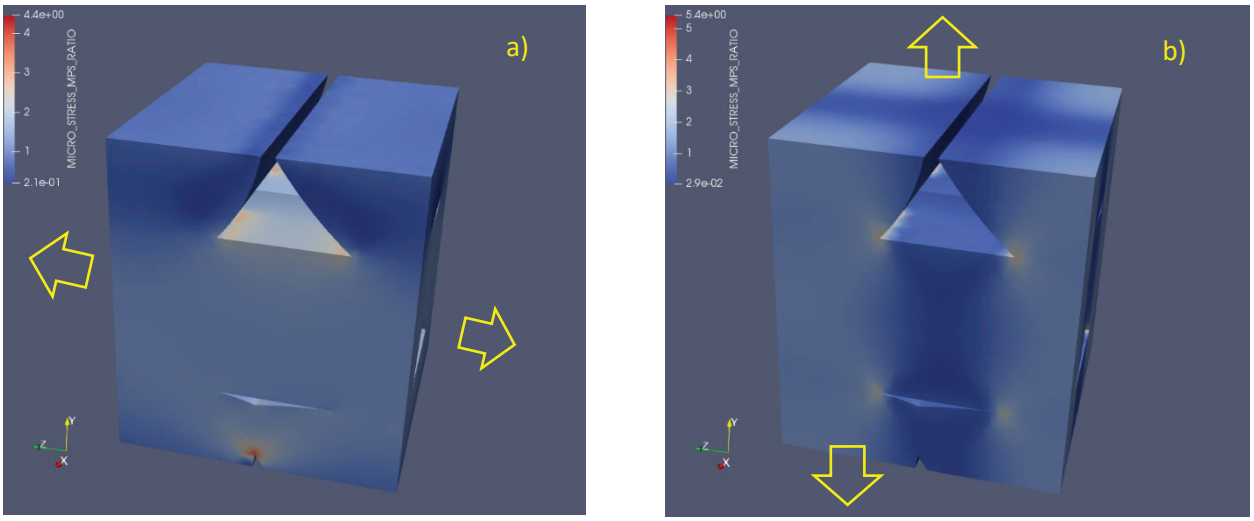

Figure 5. Microscale stress fields for loading in a) Z in direction of beads b) Y perpendicular to beads

4. Conclusion

Overall, the study assesses the prediction of mechanical properties of FDM made parts through the application of asymptotic homogenization and classical laminate theory for all-zero and 0/90 layups. Homogenization was performed for both 0 and 0/90 cases using ideal and actual RVEs. Ideal RVE was modeled as seen in slicer software and actual RVE was remodeled from microstructural images. Moreover, homogenization results from 0 layup case were used in CLT to predict properties for 0/90 layup case. The experimental setup was used to validate theoretical results. In all-zero layup, homogenization prediction using actual RVE had the least errors in 0 and 0V directions with a slight increase in 90 direction. As for 0/90 layup, homogenizing with actual RVE increases error in 0/90 and 0/90/V. CLT prediction using actual RVE results is under 8% for 0/90 layup showing best performance out of all. Overall, even though the application of actual RVE does not provide significant improvement in some cases, it provides better insight into the mechanical behavior of the RVE by calculating anisotropic RVE stiffness matrix. Visualization of microscale stress fields enhances our understanding of stress distribution on the microscale under various loading conditions.

5. References

[1] D. Bhate, Constitutive Modeling of 3D Printed FDM Parts: Part 1 (Challenges), Ansys Blog. (2016). http://www.ansys-blog.com/constitutive-modeling-of-3d-printed-fdm-parts-part-1/.

[2] E. Cuan-Urquizo, E. Barocio, V. Tejada-Ortigoza, R. Pipes, C. Rodriguez, A. Roman-Flores, Characterization of the Mechanical Properties of FFF Structures and Materials: A Review on the Experimental, Computational and Theoretical Approaches, Materials (Basel). 12 (2019) 895. doi:10.3390/ma12060895.

[3] M. Domingo-Espin, J.M. Puigoriol-Forcada, A.-A. Garcia-Granada, J. Llumà, S. Borros, G. Reyes, Mechanical property characterization and simulation of fused deposition modeling Polycarbonate parts, Mater. Des. 83 (2015) 670–677. doi:10.1016/j.matdes.2015.06.074.

[4] L. Li, Q. Sun, C. Bellehumeur, P. Gu, Composite modeling and analysis for fabrication of FDM prototypes with locally controlled properties, J. Manuf. Process. (2002). doi:10.1016/S1526-6125(02)70139-4.

[5] M. Somireddy, Mechanical Characterization of Additively Manufactured Parts by FE Modeling of Mesostructure, J. Manuf. Mater. Process. 1 (2017) 18. doi:10.3390/jmmp1020018.

[6] J. Rodriguez, Modeling the Mechanical Behavior of Fused Deposition Acrylonitrile-butadiene-styrene Polymer Components, University of Notre Dame, 1999.

[7] D. Croccolo, M. De Agostinis, G. Olmi, Experimental characterization and analytical modelling of the mechanical behaviour of fused deposition processed parts made of ABS-M30, Comput. Mater. Sci. 79 (2013) 506–518. doi:10.1016/J.COMMATSCI.2013.06.041.

[8] B. Huang, S. Singamneni, Raster angle mechanics in fused deposition modelling, J. Compos. Mater. 49 (2015) 363–383. doi:10.1177/0021998313519153.

[9] E. Cuan-urquizo, A. Bhaskar, Tema A2a Materiales : Manufactura aditiva " Micromechanics of ad ditively manufactured structures : computational and laboratory experiments ," (2018) 28–34.

[10] E. Sanchez-Palencia, Homogenization in mechanics. A survey of solved and open problems, Rend. Sem. Mat. Univ. Politec. …. 44 (1986) 1–46. doi:10.1007/BF03218609.

[11] J. Guedes, N. Kikuchi, Preprocessing and postprocessing for materials based on the homogenization method with adaptive finite element methods, Comput. Methods Appl. Mech. Eng. 83 (1990) 143–198. doi:10.1016/0045-7825(90)90148-F.

[12] J. Fish, Practical Multiscaling, 1st Edition, Wiley, 2013.

[13] B. Hassani, E. Hinton, Homogenization and Structural Topology Optimization, Springer London, London, 1999. doi:10.1007/978-1-4471-0891-7.